MICROCOPY RESOLUTION TEST CHART

NATIONAL BUREAU OF STANDARDS 1963 A

AFATL-TR-86-21

Three-Dimensional Unsteady Euler Equations Solutions on Dynamic Grids

D M BELK
J M JANUS
D L WHITFIELD

AERODYNAMICS BRANCH
AEROMECHANICS DIVISION

AD-A168 041

APRIL 1986

FINAL REPORT FOR PERIOD JANUARY-JUNE 1985

AIR FORCE ARMAMENT LABORATORY

Air Force Systems Command∗United States Air Force∗Eglin Air Force Base, Florida

86 4 30 020

NOTICE

When Government drawings, specifications, or other data are used for any purpose other than in connection with a definitely related Government procurement operation, the United States Government thereby incurs no responsibility nor any obligation whatsoever; and the fact that the Government may have formulated, furnished, or in any way supplied the said drawings, specifications, or other data, is not to be regarded by implication or otherwise as in any manner licensing the holder or any other person or corporation, or conveying any rights or permission to manufacture, use, or sell any patented invention that may in any way be related thereto.

This report has been reviewed by the Public Affairs Office (PA) and is releasable to the National Technical Information Service (NTIS). At NTIS, it will be available to the general public, including foreign nations.

This technical report has been reviewed and is approved for publication.

FOR THE COMMANDER

DONALD C. DANIEL
Chief, Aeromechanis Division

Even though this report may contain special release rights held by the controlling office, please do not request copies from the Air Force Armament Laboratory. If you qualify as a recipient, release approval will be obtained from the originating activity by DTIC. Address your request for additional copies to:

Defense Technical Information Center
Cameron Station
Alexandria, Virginia 22314

If your address has changed, if you wish to be removed from our mailing list, or if the addressee is no longer employed by your organization, please notify AFATL/DLCA , Eglin AFB FL 32542.

Copies of this report should not be returned unless return is required by security considerations, contractual obligations, or notice on a specific document.

SECURITY CLASSIFICATION OF THIS PAGE

AD-A168041

REPORT DOCUMENTATION PAGE

1a. REPORT SECURITY CLASSIFICATION Unclassified	1b. RESTRICTIVE MARKINGS
2a. SECURITY CLASSIFICATION AUTHORITY	3. DISTRIBUTION/AVAILABILITY OF REPORT Approved for public release; distribution unlimited
2b. DECLASSIFICATION/DOWNGRADING SCHEDULE	

4. PERFORMING ORGANIZATION REPORT NUMBER(S)	5. MONITORING ORGANIZATION REPORT NUMBER(S) AFATL-TR-86-21

6a. NAME OF PERFORMING ORGANIZATION Aeromechanics Division Air Force Armament Laboratory	6b. OFFICE SYMBOL (If applicable) AFATL/DLCA	7a. NAME OF MONITORING ORGANIZATION Aeromechanics Division Air Force Armament Laboratory
6c. ADDRESS (City, State and ZIP Code) EGLIN AFB FL 32542		7b. ADDRESS (City, State and ZIP Code) EGLIN AFB FL 32542
8a. NAME OF FUNDING/SPONSORING ORGANIZATION Air Force Armament Laboratory	8b. OFFICE SYMBOL (If applicable) AFATL/DLCA	9. PROCUREMENT INSTRUMENT IDENTIFICATION NUMBER

8c. ADDRESS (City, State and ZIP Code) EGLIN AFB FL 32542	10. SOURCE OF FUNDING NOS.			
	PROGRAM ELEMENT NO. 61102F	PROJECT NO. 2307	TASK NO. E1	WORK UNIT NO. 26

11. TITLE (Include Security Classification)
Three-Dimensional Unsteady Euler Equations

12. PERSONAL AUTHOR(S)
D. Belk, J. Janus, and D. Whitfield

13a. TYPE OF REPORT Final	13b. TIME COVERED FROM Jan 85 TO Jun 85	14. DATE OF REPORT (Yr., Mo., Day) April 1986	15. PAGE COUNT 30

16. SUPPLEMENTARY NOTATION
Availability of this report is specified on verso of front cover.

17. COSATI CODES			18. SUBJECT TERMS (Continue on reverse if necessary and identify by block number)
FIELD	GROUP	SUB. GR.	Computational Fluid Dynamics, Unsteady Aerodynamics, Computational Aerodynamics
0101			
2004			

19. ABSTRACT (Continue on reverse if necessary and identify by block number)

A method is presented for solving the three-dimensional unsteady Euler equations on dynamic grids based on flux vector splitting. The equations are cast in curvilinear coordinates and a finite volume discretization is used for handling arbitrary geometries. The discretized equations are solved using an explicit upwind second-order predictor corrector scheme that is stable for a CFL of 2. Characteristic variable boundary conditions are developed and used for unsteady impermeable surfaces and for the far-field boundary. Dynamic-grid results are presented for an oscillating airfoil and for a store separating from a reflection plate. For the cases considered of stores separating from a reflection plate, the unsteady aerodynamic forces on the store are significantly different from forces obtained by steady-state aerodynamics with the body inclination angle changed to account for plunge velocity.

20. DISTRIBUTION/AVAILABILITY OF ABSTRACT UNCLASSIFIED/UNLIMITED ☒ SAME AS RPT. ☐ DTIC USERS ☐	21. ABSTRACT SECURITY CLASSIFICATION Unclassified	
22a. NAME OF RESPONSIBLE INDIVIDUAL DAVE M. BELK	22b. TELEPHONE NUMBER (Include Area Code) (904) 882-5652	22c. OFFICE SYMBOL DLCA

DD FORM 1473, 83 APR   EDITION OF 1 JAN 73 IS OBSOLETE.   UNCLASSIFIED

SECURITY CLASSIFICATION OF THIS PAGE

11. TITLE (CONCLUDED)

Solutions on Dynamic Grids

PREFACE

This work was conducted during the period January to June 1985 by the Aerodynamics Branch, Aeromechanical Division, Air Force Armament Laboratory, Eglin Air Force Base, Florida. The program manager was Dave Belk.

Accesion For	
NTIS CRA&I	☑
DTIC TAB	☐
Unannounced	☐
Justification	
By	
Distribution /	
Availability Codes	
Dist	Avail and / or Special
A-1	

QUALITY INSPECTED 3

iii
(The reverse of this page is blank)

TABLE OF CONTENTS

LIST OF FIGURES

SECTION I
INTRODUCTION

An example of an important application of three-dimensional Euler equation solutions on dynamic grids is that of transonic flow about non-stationary stores. Unsteady aerodynamic information is extremely difficult and costly to obtain in wind tunnel experiments, particularly in the transonic regime. Consequently, it is important to know when steady-state, quasi-steady, or true unsteady aerodynamic information is required. Computational fluid dynamics (CFD) has matured to the point where it can be used to assist in deciding the conditions for which steady or unsteady information is needed, as well as being itself a source for providing such information.

To compute the flow of a store released from an aircraft, it is desirable to solve the unsteady Euler equations on a grid that moves with the store along its trajectory. The purpose of this paper is to solve the three-dimensional unsteady Euler equations on a time-dependent grid. The computations presented here are for bodies whose motion is prescribed. As the solution advances in time, body motion could be determined from the Euler equations by using force and moment coefficients obtained from the Euler solution in the dynamic equations of motion for the body to determine the trajectory of the body. The objective of this report is to present and verify dynamic-grid Euler equations computations.

The Euler equations solution method used is similar to that presented by Janus, Reference 1. It is a finite volume, flux-vector split, second-order explicit scheme, that can use local time stepping with CFL ≤ 2 for steady-state computations, Reference 2. The flux vectors at cell faces are determined differently in the present method. In References 1 and 2 the flux vectors at cell faces depend on a cell face eigenvalue that was determined from information resulting from averaging dependent variables on either side of the cell face. Due to the splitting, each flux vector is the sum of three subvectors, each of which has an eigenvalue as a coefficient. The cell face eigenvalue, computed as described above, was used to compute a flux vector; however, the remaining portion of the flux vector was computed with information from the

1

appropriate direction as dictated by the sign of the eigenvalue. In the present method, each subvector of a flux vector is computed on either side of a cell face by extrapolating the dependent variables from either side of a cell face. An eigenvalue on either side of a cell face is computed in like manner. The flux vector at a cell face is then formed by summing the subvectors on either side of a cell face by appropiately taking into account the sign of the eigenvalues. This method requires less storage and executes more quickly than the previous. It also totally eliminates upstream propagation of information in supersonic regions. Experience with this technique has shown that the ringing downstream of shocks characteristic of the previous method is greatly reduced. A disadvantage of the method is that in practice it frequently requires a slightly lower CFL number for stability than the previous method.

Characteristic variable boundary conditions (Reference 1) are used on all boundaries with the exception of the reflection plate used in the moving store calculations. On the reflection plate, reflection plane boundary conditions are used.

SECTION II
ALGORITHM

1. BASIC EQUATIONS

The conservation law form of the Euler equations in Cartesian coordinates x, y, and z is

$$\frac{\partial \bar{q}}{\partial t} + \frac{\partial f}{\partial x} + \frac{\partial g}{\partial y} + \frac{\partial h}{\partial z} = 0 \qquad (1)$$

where

$$\bar{q} = [\rho, \rho u, \rho v, \rho w, e]^T$$

$$f = [\rho u, \rho u^2 + p, \rho u v, \rho u w, u(e+p)]^T$$

$$g = [\rho v, \rho u v, \rho v^2 + p, \rho v w, v(e+p)]^T$$

$$h = [\rho w, \rho u w, \rho v w, \rho w^2 + p, w(e+p)]^T$$

$$p = (\gamma - 1)[e - \frac{1}{2}\rho(u^2 + v^2 + w^2)]$$

Using time-dependent curvilinear coordinates defined by

$$\xi = \xi(x, y, z, t)$$

$$\eta = \eta(x, y, z, t)$$

$$\zeta = \zeta(x, y, z, t) \quad .$$

$$\tau = t,$$

3

Equation (1) may be transformed to (Reference 3)

$$\frac{\partial Q}{\partial \tau} + \frac{\partial F}{\partial \xi} + \frac{\partial G}{\partial \eta} + \frac{\partial H}{\partial \zeta} = 0 \qquad (2)$$

where

$$Q = J[\rho, \rho u, \rho v, \rho w, e]^T$$

$$F = J[\rho U, \rho u U + \xi_x p, \rho v U + \xi_y p, \rho w U + \xi_z p, U(e+p) - \xi_t p]^T$$

$$G = J[\rho V, \rho u V + \eta_x p, \rho v V + \eta_y p, \rho w V + \eta_z p, V(e+p) - \eta_t p]^T$$

$$H = J[\rho W, \rho u W + \zeta_x p, \rho v W + \zeta_y p, \rho w W + \zeta_z p, W(e+p) - \zeta_t p]^T$$

$$J = x_\xi(y_\eta z_\zeta - z_\eta y_\zeta) - y_\xi(x_\eta z_\zeta - z_\eta x_\zeta) + z_\xi(x_\eta y_\zeta - y_r \zeta)$$

$$\xi_x = J^{-1}(y_\eta z_\zeta - z_\eta y_\zeta) \qquad \xi_y = J^{-1}(z_\eta x_\zeta - x_\eta z_\zeta)$$

$$\eta_x = J^{-1}(z_\xi y_\zeta - y_\xi z_\zeta) \qquad \eta_y = J^{-1}(x_\xi z_\zeta - z_\xi x_\zeta)$$

$$\zeta_x = J^{-1}(y_\xi z_\eta - z_\xi y_\eta) \qquad \zeta_y = J^{-1}(x_\eta z_\xi - z_\eta x_\xi)$$

$$\xi_z = J^{-1}(x_\eta y_\zeta - y_\eta x_\zeta) \qquad \xi_t = -x_\tau \xi_x - y_\tau \xi_y - z_\tau \xi_z$$

$$\eta_z = J^{-1}(x_\zeta y_\xi - y_\zeta x_\xi) \qquad \eta_t = -x_\tau \eta_x - y_\tau \eta_y - z_\tau \eta_z$$

$$\zeta_z = J^{-1}(x_\xi y_\eta - y_\xi x_\eta) \qquad \zeta_t = -x_\tau \zeta_x - y_\tau \zeta_y - z_\tau \zeta_z$$

$$U = \xi_x u + \xi_y v + \xi_z w + \xi_t$$

$$V = \eta_x u + \eta_y v + \eta_z w + \eta_t$$

$$W = \zeta_x u + \zeta_y v + \zeta_z w + \zeta_t$$

A finite volume discretization of Equation (2) balances the increase of the conserved quantity in a computational cell, or volume, with the flux of the quantity through the surface of the cell. Figure 1 depicts a portion of the computational domain with a typical cell labeled. Assuming the dependent variables are constant in the interior of cell i, j, k, and that the flux vectors F, G, and H are constant over the constant ξ, constant η and constant ζ surfaces of the cell, respectively, an explicit discretization of Equation (2) is

$$(Q^{n+1}_{i,j,k} - Q^{n}_{i,j,k})\Delta\xi\Delta\eta\Delta\zeta + (F^{n}_{i+\frac{1}{2},j,k} - F^{n}_{i-\frac{1}{2},j,k})\,\Delta\eta\Delta\zeta\Delta\tau$$

$$+ (G^{n}_{i,j+\frac{1}{2},k} - G^{n}_{i,j-\frac{1}{2},k})\Delta\xi\Delta\zeta\Delta\tau + (H^{n}_{i,j,k+\frac{1}{2}} - H^{n}_{i,j,k-\frac{1}{2}})\Delta\xi\Delta\eta\cdots = 0 \tag{3}$$

This can be rewritten as

$$\frac{\Delta Q_{i,j,k}}{\Delta\tau} + \frac{\delta F_i}{\Delta\xi} + \frac{\delta G_j}{\Delta\eta} + \frac{\delta H_k}{\Delta\zeta} = 0 \tag{4}$$

Note that any algorithm written in this form is conservative as long as the fluxes are single-valued functions of the cell faces.
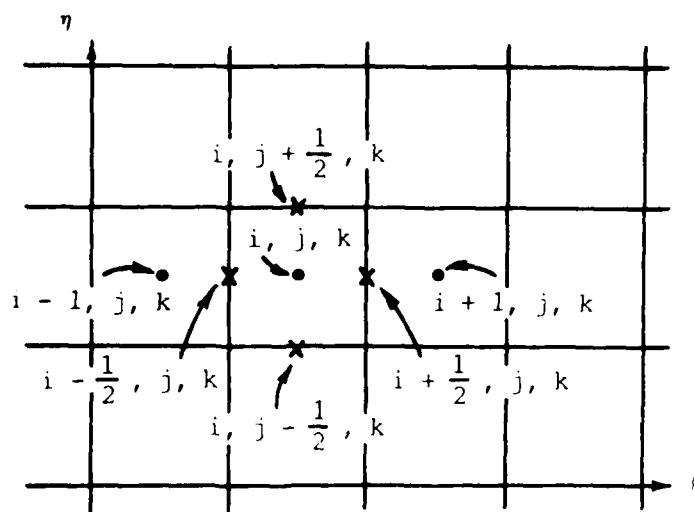
ζ = Constant Plane

Figure 1. Computational Grid

2. FLUX SPLITTING

Hyperbolic partial differential equations, such as the Euler equations, are characterized by the existence of a limited domain of dependence. The solution at a point does not depend on every other point in the field; this means that information travels only in certain characteristic directions. Numerical schemes intended to solve hyperbolic equations are usually enhanced by insuring that the numerical method propagates information in the direction specified by the partial differential equation. This can be done by using an upwind method, or one in which the difference operator is taken in the direction from which the information should come. Stability properties are often improved by upwinding, and it is usually unnecessary to add smoothing terms or artificial viscosity to an upwind method.

The three-dimensional Euler equations, Equation (2), are a hyperbolic system of five equations and hence have five characteristic velocities in each of the three spatial directions. These characteristic velocities are determined from the quasilinear form of Equation (2),

$$\frac{\partial Q}{\partial \tau} + A\frac{\partial Q}{\partial \xi} + B\frac{\partial Q}{\partial \eta} + C\frac{\partial Q}{\partial \zeta} = 0 \qquad (5)$$

where the matrices A, B, and C are given by

$$A = \frac{\partial F}{\partial Q}, \qquad B = \frac{\partial G}{\partial Q}, \qquad C = \frac{\partial H}{\partial Q}$$

The eigenvalues of A are the characteristic velocities in the ξ direction; the eigenvalues of B are the characteristic velocities in the η direction; and similarly the eigenvalues of C are the characteristic velocities in the ζ direction.

Since F, G, and H are identical except that where ξ appears in F, η will appear in G and ζ will appear in H, extra writing can be avoided by letting K represent either F, G, or H, and k represent either ξ, η, or ζ.
Then define

$$\bar{K} = \frac{\partial K}{\partial Q} \qquad (6)$$

which corresponds to A, B, or C depending on the meaning of K. The eigenvalues of the matrix K are

$$\lambda_k^1 = \lambda_k^2 = \lambda_k^3 = k_x u + k_y v + k_z w + k_t = \beta_k$$

$$\lambda_k^4 = \beta_k + c|\nabla k| = \beta_k + c(k_x^2 + k_y^2 + k_z^2)^{\frac{1}{2}} \qquad (7)$$

$$\lambda_k^5 = \beta_k - c|\nabla k|$$

where c is the speed of sound.

It is possible to split the flux vector K into three parts, one corresponding to each of the distinct eigenvalues of K given above. (For the details of this splitting, see Reference 1). The flux vector K is then written as

$$K = \lambda_k^1 K_1 + \lambda_k^4 K_4 + \lambda_k^5 K_5 \qquad (8)$$

where

$$K_1 = J\frac{\gamma-1}{\gamma}\begin{Bmatrix} \rho \\ \rho u \\ \rho v \\ \rho w \\ \frac{\rho}{2}(u^2+v^2+w^2) \end{Bmatrix} \qquad K_4 = \frac{J}{2\gamma}\begin{Bmatrix} \rho \\ \rho u+\rho c\bar{k}_x \\ \rho v+\rho c\bar{k}_y \\ \rho w+\rho c\bar{k}_z \\ e+p+\rho c\tilde{\theta}_k \end{Bmatrix}$$

7

$$K_5 = \frac{J}{2\gamma} \begin{bmatrix} \rho \\ \rho u - \rho c \bar{k}_x \\ \rho v - \rho c \bar{k}_y \\ \rho w - \rho c \bar{k}_z \\ e + p - \rho c \bar{\theta}_k \end{bmatrix} \qquad (9)$$

and

$$\bar{k}_x = \frac{k_x}{|\nabla k|} = \frac{k_x}{(k_x^2 + k_y^2 + k_z^2)^{\frac{1}{2}}}$$

$$\bar{k}_y = \frac{k_y}{|\nabla k|}$$

$$\bar{k}_z = \frac{k_z}{|\nabla k|}$$

$$\bar{\theta}_k = \bar{k}_x u + \bar{k}_y v + \bar{k}_z w.$$

The sign of λ_k^ℓ in Equation (8) determines from which direction information should be used to determine the corresponding portion of the flux, K_ℓ.

3. NUMERICAL IMPLEMENTATION

For the finite volume discretization, Equation (4), the dependent variables are stored at cell centers, but the fluxes are required at cell faces. Therefore, some type of interpolation or extrapolation must be used to determine the fluxes. The signs of the eigenvalues at the faces should determine the direction of the extrapolation to be used, but note that there is still some ambiguity, since the eigenvalues themselves may be calculated in several different ways at cell faces. Whitfield and Janus (Reference 2) computed the eigenvalues at a face from the average of dependent variables in the two cells sharing the face. The present scheme uses a different approach. The scheme reported here calculates a set of left eigenvalues, $\lambda_k^\ell(Q^L)$, and left split

fluxes, $K_\ell(Q^L)$ from dependent variables extrapolated from cell centers left of the face, Q^L, and it also calculates a set of right eigenvalues, $\lambda_k^\ell (Q^R)$, and right split fluxes, $K_\ell (Q^R)$, from dependent variables extrapolated from cell centers right of the face, Q^R. The flux at the face is then set to

$$
K(Q^L, Q^R) = \sum_{\ell=1,4,5} [\frac{1}{2}(\lambda_k^\ell (Q^L) + |\lambda_k^\ell(Q^L)|)K_\ell (Q^L)
$$

$$
+ \frac{1}{2}(\lambda_k^\ell(Q^R) - |\lambda_k^\ell(Q^R)|)K_\ell(Q^R)] \tag{10}
$$

Note that if a left and right eigenvalue have different signs, then the corresponding split flux may be either summed from both sides, if the sign changes from positive to negative, or from neither side, if the sign changes from negative to positive.

The extrapolation of dependent variables is chosen such that the algorithm is a finite volume version of the Warming-Beam upwind scheme, Reference 6. This predictor-corrector scheme is second-order accurate in time and space, and is stable for CFL numbers less than two. Three flux balances are performed, requiring two different dependent variable extrapolations. The one-point extrapolation in the ξ direction is

$$
\bar{Q}^L_{i+\frac{1}{2},j,k} = Q^n_{i,j,k}
$$

$$
\tag{11}
$$

$$
\bar{Q}^R_{i+\frac{1}{2},j,k} = Q^n_{i+1,j,k}
$$

The two-point extrapolation in the ξ direction is

$$
\hat{Q}^L_{i+\frac{1}{2},j,k} = 2Q^n_{i,j,k} - Q^n_{i-1,j,k}
$$

$$
\tag{12}
$$

$$
\hat{Q}^R_{i+\frac{1}{2},j,k} = 2Q^n_{i+1,j,k} - Q^n_{i+2,j,k}
$$

9

Similar extrapolations are used in the η and ζ directions. Taking $\Delta\xi = \Delta\eta = \Delta\zeta$, the predictor is

$$\bar{Q}_{i,j,k} = Q^n_{i,j,k} - \Delta\tau_{i,j,k}[\delta\bar{F}_i + \delta\bar{G}_j + \delta\bar{H}_k] \qquad (13)$$

where

$$\delta\tilde{F}_i = F(\bar{Q}^L_{i+\frac{1}{2},j,k}, \bar{Q}^R_{i+\frac{1}{2},j,k}) - F(\bar{Q}^L_{i-\frac{1}{2},j,k}, \bar{Q}^R_{i-\frac{1}{2},j,k})$$

and $\delta\tilde{G}_j$ and $\delta\tilde{H}_k$ are evaluated similarly.

The corrector is written as

$$Q^{n+1}_{i,j,k} = Q^n_{i,j,k} - \frac{\Delta\tau_{i,j,k}}{2}[\delta\hat{F}_i + \delta\hat{G}_j + \delta\hat{H}_k]$$

$$\qquad (14)$$

$$- \frac{\Delta\tau_{i,j,k}}{2}[\delta\tilde{F}_i + \delta\tilde{G}_j + \delta\tilde{H}_k]$$

where

$$\delta\hat{F}_i = F(\hat{Q}^L_{i+\frac{1}{2},j,k}, \hat{Q}^R_{i+\frac{1}{2},j,k}) - F(\hat{Q}^L_{i-\frac{1}{2},j,k}, \hat{Q}^R_{i-\frac{1}{2},j,k})$$

and $\delta\hat{G}_j$ and $\delta\hat{H}_k$ similarly are flux differences using two-point dependent variable extrapolations. $\delta\tilde{F}_i$, $\delta\tilde{G}_j$, and $\delta\tilde{H}_k$ represent differences of fluxes evaluated using a one-point extrapolation of the predicted variables.

The time step $\Delta\tau_{i,j,k}$ is given by

$$\Delta\tau_{i,j,k} = \frac{\Delta\tau^\xi_{i,j,k}\Delta\tau^\eta_{i,j,k}\Delta\tau^\zeta_{i,j,k}}{\Delta\tau^\xi_{i,j,k}\Delta\tau^\eta_{i,j,k} + \Delta\tau^\xi_{i,j,k}\Delta\tau^\zeta_{i,j,k} + \Delta\tau^\eta_{i,j,k}\Delta\tau^\zeta_{i,j,k}}$$

$$\qquad (15)$$

where

$$\Delta\tau^k_{i,j,k} = \frac{CFL\Delta k}{\max|\lambda^1_k|} \qquad (16)$$

10

for $k = \xi, \eta$, and ζ. When time accuracy is not required (steady state) the
maximum time step for each individual cell is used where CFL $\leq$ 2. This is done
to accelerate convergence by enabling every cell to advance in time as fast as
possible. The edge cells (those in the domain adjacent to a boundary) are only
first-order accurate and stable for a CFL $\leq$ 1, consequently the time steps for
these cells are reduced accordingly. In situations where a time accurate
solution is desired, such as in some dynamic grid applications, the minimum of
all the local time steps is selected for use at all cells. This enables the
solution to advance at the same time in every cell, although restricting the
time step to that of the slowest cell. This method of selecting the time step
is referred to as minimum time stepping.

4. BOUNDARY CONDITIONS

Consistent with the impetus leading to the flux split form of the Euler
equations, i.e., honoring propagation directions, a set of boundary conditions
has been developed, referred to as the characteristic variable boundary condi-
tions (CVBC), Reference 2. The CVBC presented in Reference 2 are formulated
for stationary grids. Some minor adjustments to these equations are required
to establish a valid set of CVBC for the dynamic grid case.

The characteristic variables are constructed, Reference 1, using the matrix
of eigenvectors of the flux Jacobian and the non-conservative dependent vari-
able vector. Since in the dynamic grid derivation neither the eigenvectors or
dependent variables are altered, Reference 1, the characteristic variables
remain unchanged. Consequently the equations corresponding to the cases
described in Reference 2 are all valid except for the case of the impermeable
surface. This case will be reformulated for the dynamic grid application.

The impermeable surface case is characterized by the first three eigen-
values equal to zero, the fourth positive, and the fifth negative. For this

11

case no flow through the surface must be specified, replacing one of the characteristic variable relation equations yielding

$$\left[k_x\left(\rho - \frac{p}{c_o^2}\right) + k_z v - k_y w\right]_b = \left[k_x\left(\rho - \frac{p}{c_o^2}\right) + k_z v - k_y w\right]_r \quad (17a)$$

$$\left[k_y\left(\rho - \frac{p}{c_o^2}\right) - k_z u + k_x w\right]_b = \left[k_y\left(\rho - \frac{p}{c_o^2}\right) - k_z u + k_x w\right]_r \quad (17b)$$

$$\left[k_z\left(\rho - \frac{p}{c_o^2}\right) + k_y u - k_x v\right]_b = \left[k_z\left(\rho - \frac{p}{c_o^2}\right) + k_y u - k_x v\right]_r \quad (17c)$$

$$\left[k_x u + k_y v + k_z w + k_t\right]_b = 0 \quad (17d)$$

$$\left[\frac{p|\nabla k|}{\rho_o c_o} \mp (k_x u + k_y v + k_z w)\right]_b = \left[\frac{p|\nabla k|}{\rho_o c_o} \mp (k_x u + k_y v + k_z w)\right]_r \quad (17e)$$

where the r subscripts refer to a reference value, which is selected as the center of the first cell from the boundary, and the b subscripts refer to boundary values. Solving Equations 17d,e for Δp yields

$$\Delta p = p_b - p_r = \mp \rho_o c_o (\bar{k}_x u_r + \bar{k}_y v_r + \bar{k}_z w_r + \bar{k}_{t,b}) \quad (18a)$$

The other relations can be obtained by solving Equations (17a,b,c,d) simultaneously yielding

$$\Delta u = u_b - u_r = -\bar{k}_x \frac{\Delta p}{\rho_o c_o} \quad (18b)$$

$$\Delta v = v_b - v_r = -\bar{k}_y \frac{\Delta p}{\rho_o c_o} \quad (18c)$$

$$\Delta w = w_b - w_r = -\bar{k}_z \frac{\Delta p}{\rho_o c_o} \quad (18d)$$

$$\Delta \rho = \rho_b - \rho_r = \frac{\Delta p}{c_o^2} \quad (18e)$$

The minus and plus signs in Equations (18a) correspond to the location of the point r. If the point r is in the positive k direction from the boundary then the minus sign is used, and if it is in the negative direction then the plus sign is used.

12

SECTION III
RESULTS

Dynamic-grid computations were performed for the following configurations: (a) plunging and oscillating airfoils, (b) plunging wings, (c) horizontally launched missile (or store), and (d) vertically launched store from a reflection plate. The plunging airfoil and wing cases were run for the special case of constant velocity plunge in order to check the dynamic-grid code. A constant velocity plunge corresponds to a stationary solution at some particular angle of attack. The constant velocity plunge solutions were compared with steady-grid angle of attack solutions to insure that both solutions were identical, which they were. The same was done for the horizontally launched missile. In one case the missile was launched into still air and then the solution was compared with a solution for a stationary missile with the air flowing past. These results were reported in Reference 1. The same numerical experiment was also performed for a store in constant velocity vertical plunge and a stationary store at angle of attack. Again the solutions were identical.

The cases selected are the solution for an oscillating airfoil and the solution for a vertically launched store from a reflection plate. The oscillating airfoil was investigated because of the need to determine whether the phase was being computed correctly. Experimental data are available for an NACA 0012 airfoil, Reference 5, consequently this airfoil was selected. The experiment consisted of the harmonic pitch oscillation of a NACA 0012 airfoil about the quarter chord point. Figure 1 is the result obtained from the harmonic oscillation using a reduced frequency of 0.2156 and oscillating $\pm$ 2.51° about a mean alpha of 0.016° in a uniform Mach 0.755 flow. In an attempt to isolate the phase shift of the lift curve, the normalized lift curves of the numerical solution and experimental data, Reference 3, are shown in Figure 2. It is evident from this figure that the correct phase is calculated. The lift curves could not be directly compared because the numerical solution was obtained using a rather coarse grid, consequently the resolution of the values of lift and drag is not adequate.

13

NACA 0012 AIRFOIL PITCH OSCILLATION
(M=.755. k=.2156, -2.494°≤α≤ 2.526°)

NORMALIZED ALPHA ————————————
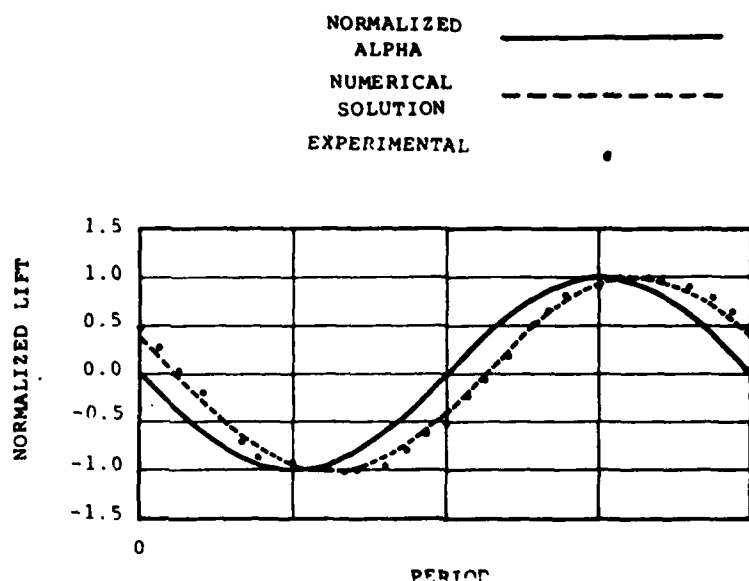
NUMERICAL SOLUTION — — — — — — —

EXPERIMENTAL •

Figure 2. Phase Shift (computed and experimental)

Finer grid steady-state solutions were obtained and compared to previous lift and drag Euler solutions to make sure the present code produces acceptable results for steady state. For example, for $M_\infty = 0.8$ and $\alpha = 1.25^o$ the lift and drag coefficients are $C_L = 0.3796$ and $C_D = 0.0211$, whereas Anderson, Thomas, and Van Leer, Reference 6, give $C_L = 0.3740$ and $C_D = 0.0232$.

The second case presented here is that of a store launched vertically from a reflection plate. There appear to be no experimental data available for stores moving in the vicinity of wings or other stores. There are steady-state data available for a store located at various positions relative to a reflection plate, Reference 7. A grid with 60 points in the streamwise direction, 10 points in the radial direction, and 30 points in the circumferential direction was used to obtain comparisons with the steady experimental data for $M_\infty =1.41$ and a zero store angle of attack with respect to the reflection plate. The model geometry and grid are illustrated in Figure 3. A plane of symmetry

14

perpendicular to the reflection plate and bisecting the store was taken advantage of to half the size of the problem. A comparison is presented in Figure 4 of computed and measured store surface pressure distributions for a store nose to reflection plate separation distance of 10.07 percent of the store length. The dip in the C_p curve near the nose is due to the reflection of the shock emanating from the store nose. Although viscous effects are not accounted for on either the store or reflection plate in the present computations, good qualitative agreement is obtained between the computed and measured steady-state data.

BOUNDARY-LAYER BYPASS PLATE

MODEL and INTEGRAL STING

AIRSTREAM
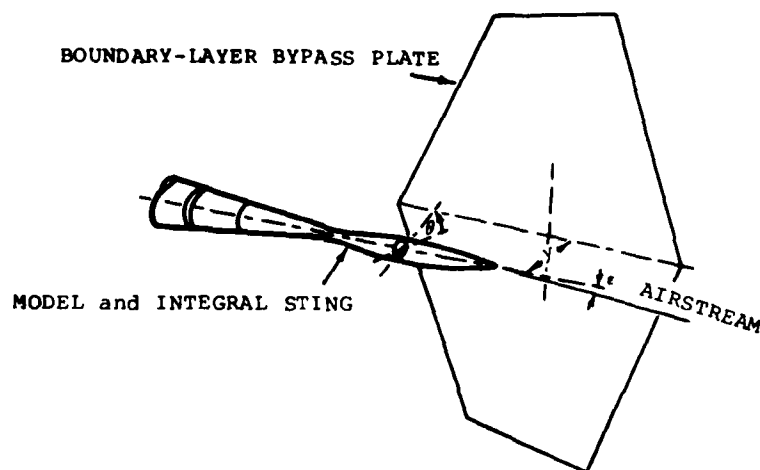
Figure 3 (a). Perspective View of Test Setup
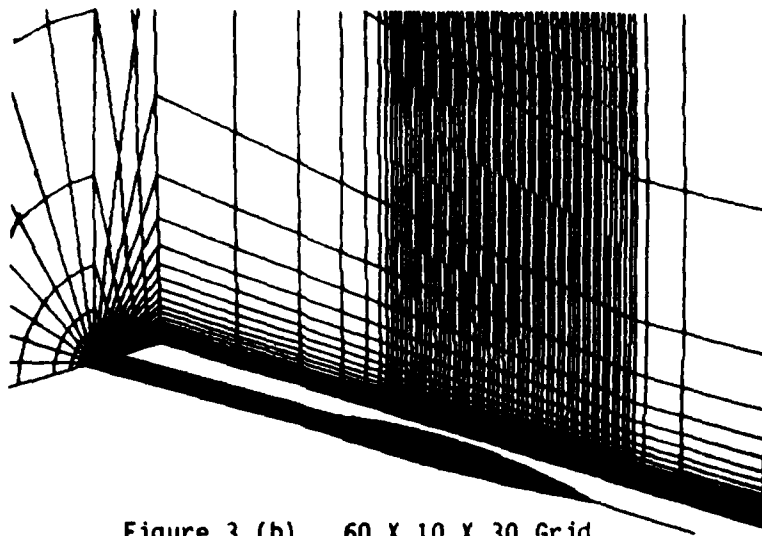
Figure 3 (b). 60 X 10 X 30 Grid

15
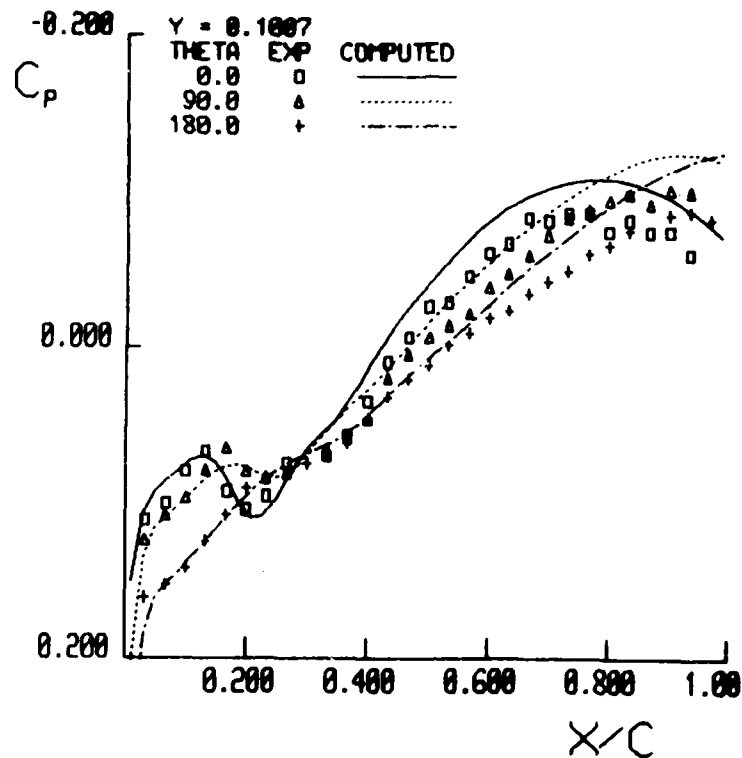
Figure 4. Computed and Experimental Store Surface Pressures

To help assess the importance of unsteady aerodynamics during store separation, dynamic-grid Euler solutions were obtained for the store discussed above when launched from the 10.07 percent location in a direction perpendicular to and away from the plate. The procedure used for this calculation was to first calculate the initial steady-state flow field with the store at the 10.07 percent location. The plunge velocity of the store away from the wall was then suddenly set to a predetermined value and held constant thereafter. Present-day store separation analyses typically use steady aerodynamics with a correction to the store angle of attack to account for the unsteady store motion. The geometric angle of attack of the store, i.e. the pitch angle ε in Figure 3(a), is incremented by the effective angle of attack due to the instantaneous

16

store plunge velocity. In other words, if the free stream velocity is U_∞ and if the store has a plunge velocity of v, then the aerodynamic forces for this case are usually obtained from steady aerodynamics with ε incremented by an amount given by

$$\alpha_u = \tan^{-1} \frac{v}{U_\infty} \qquad (19)$$

To evaluate the validity of this approximation, a set of steady computations were performed for a store with $\varepsilon = 3$ degrees and compared with two unsteady dynamic-grid computations. For these calculations, a 60 by 10 by 15 grid was used. The first dynamic-grid computation had $\varepsilon = 0$ degrees and a downward velocity such that the effective angle of attack due to the velocity, α_u, was 3 degrees. The second dynamic-grid computation had $\varepsilon = 2$ degrees and an effective angle of attack increment due to velocity of one degree. As explained earlier, the aerodynamics for both of these unsteady cases would normally be modelled in a store separation analysis by a steady-state condition with $\varepsilon = 3$ degrees. A comparison of the store pressure distribution along the $\theta = 0$ plane (see Figure 3) for the steady and two unsteady cases is presented in Figure 5. The reflection plate pressure distribution for the same conditions is given in Figure 6. From the figures it is apparent that a noticeable difference does exist between the steady and unsteady cases particularly during the initial moments of the store motion. Note that the pressures on the store ahead of the reflected shock for the $\alpha_u = 1$ degree case quickly become indistinguishable for the steady results, but the $\alpha_u = 3$ case shows a larger difference. The greatest difference in results is due to the position of the reflected shock. A comparison of normal force and pitching moment coefficients is given in Figure 7. Figure 7(a) shows a spike in the normal force coefficient at the first time step which is due to apparent mass effects from the impulsive change in velocity. This is a transient effect which decays quickly. After the decay of the large transient due to store acceleration, a difference between the steady and unsteady cases still exists. This is due at least in part to the lag in the reflected shock's position for the unsteady case.
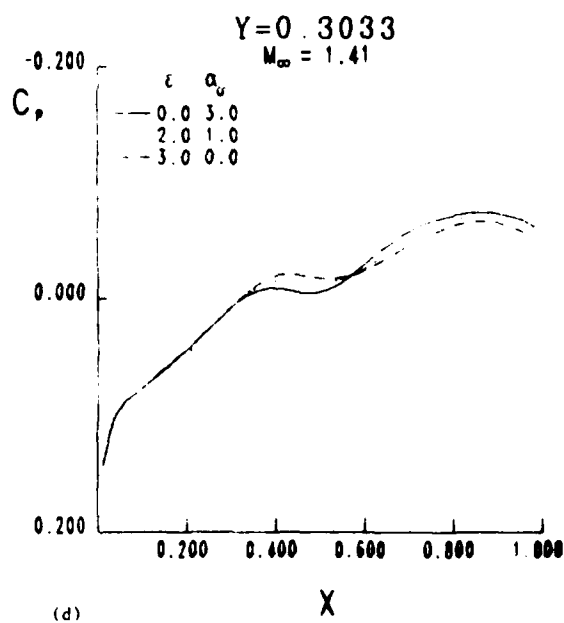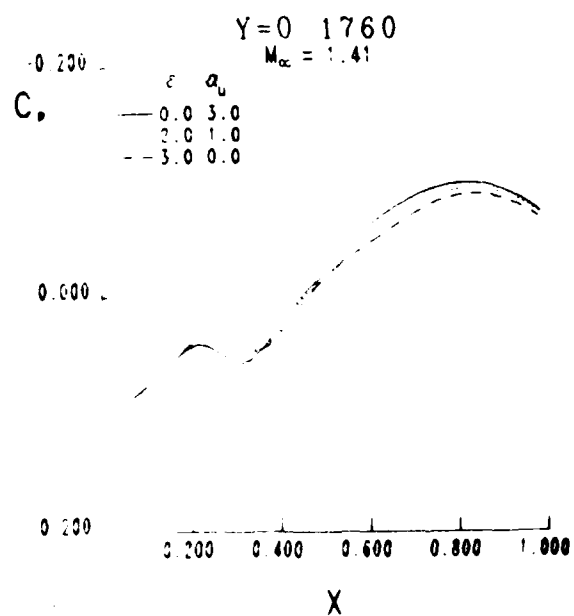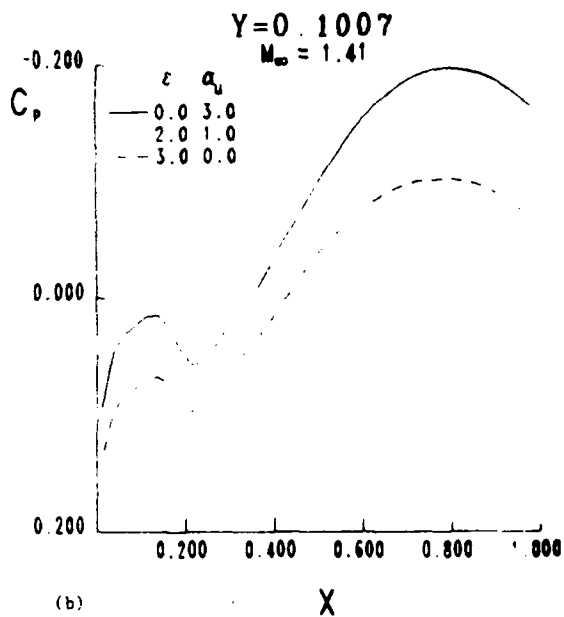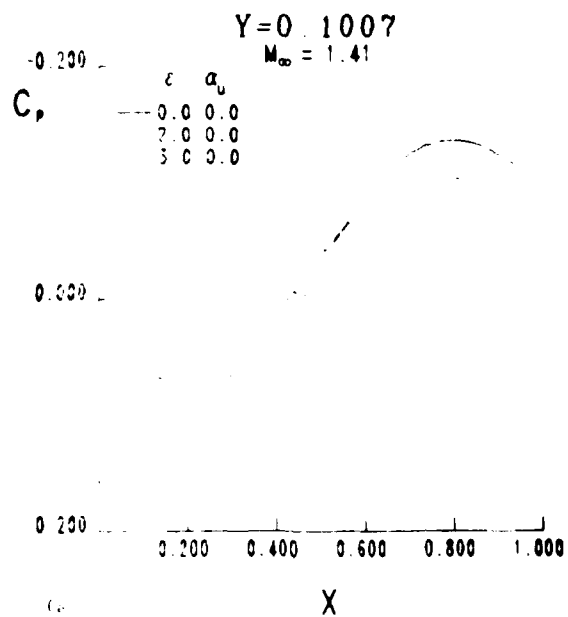
17

Figure 5. Comparison of Store Surface Pressure Along θ = 0 for Unsteady
Store Motion and For Steady Store at Equivalent Angle of Attack
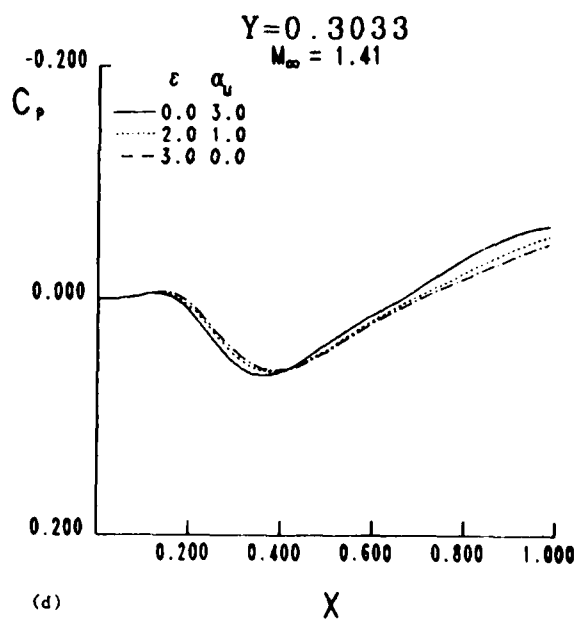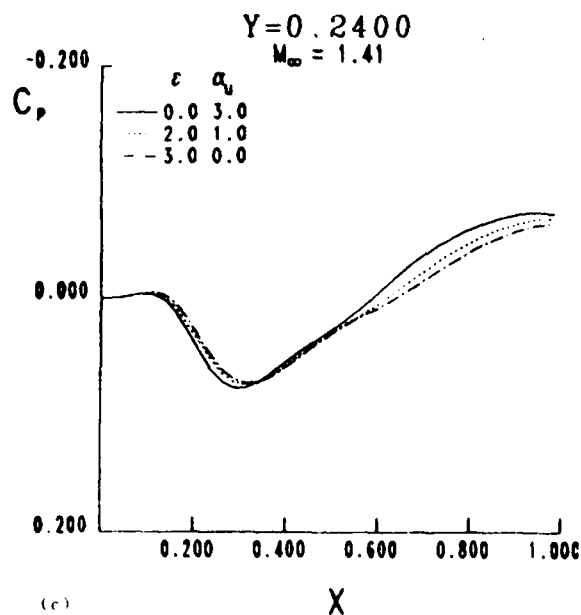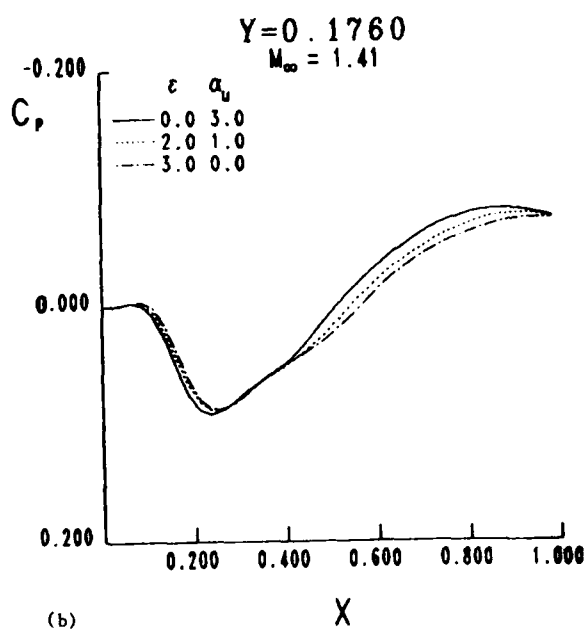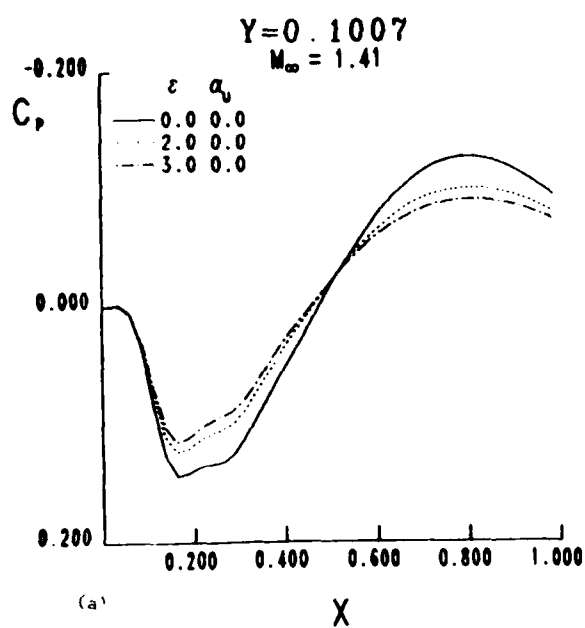
18

Figure 6. Comparison of Reflection Plate Pressures For Unsteady Store
Motion and For Steady Store Equivalent Angle of Attack

NORMAL FORCE

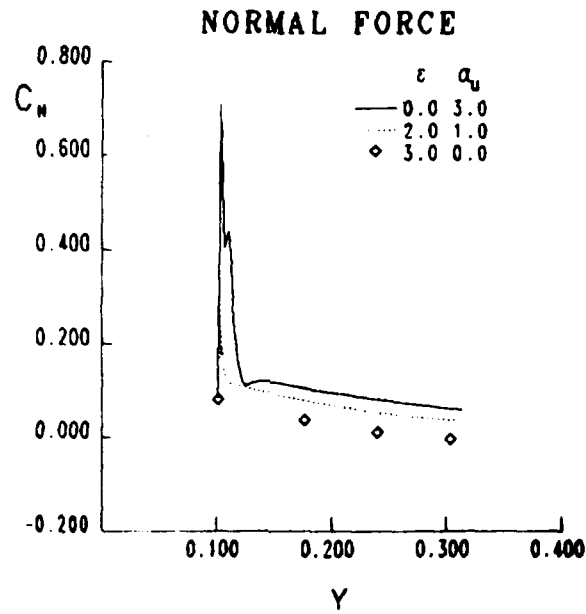Figure 7(a). Store Normal Force Coefficient
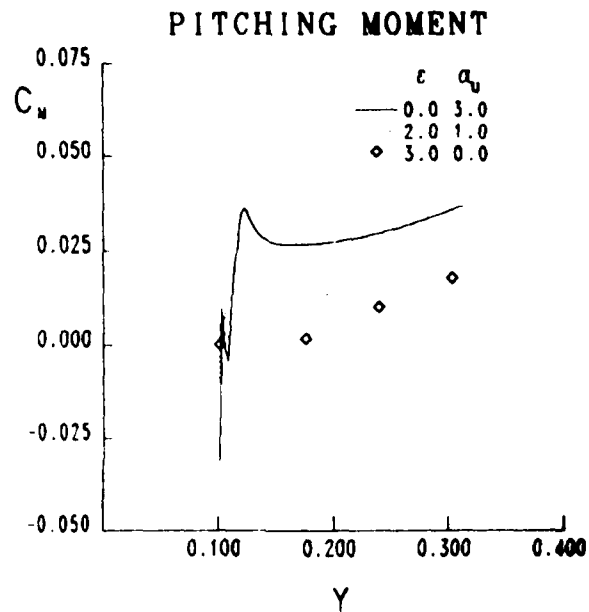
PITCHING MOMENT

Figure 7 (b). Coefficient of Pitching Moment About 59.8 Percent

20

These results illustrate the difference in aerodynamic forces for a pres-
cribed store trajectory. It is possible to determine the store trajectory
using forces and moments obtained from the Euler equations, as Mastin did.
(Reference 8) To determine the significance of true unsteady aerodynamics
to store separation, the rigid body equations of motion should be solved
using both the unsteady and the steady aerodynamics so that the difference
in the store trajectory can be seen.

SECTION IV
CONCLUDING REMARKS

A method was presented for solving the three-dimensional unsteady Euler equations on dynamic grids based on flux vector splitting. The equations were cast in curvilinear coordinates and a finite volume discretization was used for handling arbitrary geometries. The discretized equations were solved using an explicit upwind second-order predictor-corrector scheme that is stable for a CFL of 2. Characteristic variable boundary conditions were developed and used for unsteady impermeable surfaces and for the far-field boundary. Dynamic-grid results were presented for an oscillating airfoil and for a store separating from a reflection plate.

It was determined that for the cases considered of stores separating from a reflection plate that the unsteady aerodynamic forces on the store are significantly different from forces obtained by steady-state aerodynamics with the body inclination angle changed to account for plunge velocity.

References

1. Janus, J. M. "The Development of a Three-Dimensional Split Flux Vector Euler Solver with Dynamic Grid Applications," M.S. Thesis, Mississippi State University, Mississippi State, MS, August 1984.

2. Whitfield, D. L. and Janus, J. M. "Three-Dimensional Unsteady Euler Equations Solution Using Flux Vector Splitting," AIAA Paper No. 84-1552, June 1984.

3. Pulliam, T. H. and Steger, J. L., "On Implicit Finite-Difference Simulations of Three Dimensional Flow," AIAA Paper No. 78-10, January 1978.

4. Warming, R. F. and Beam, R. M., "Upwind Second-Order Difference Schemes and Applications in Aerodynamic Flows," AIAA Journal, Vol. 14, No. 9, September 1976, pp. 1241 - 1249.

5. Landon, R. H., ARA, "NACA 0012. Oscillatory and Transient Pitching," Compendium of Unsteady Aerodynamic Measurements, AGARD R-702, 1982.

6. Anderson, W. K., Thomas, J. L., and Van Leer, B., "A Comparison of Finite Volume Flux Vector Splittings for the Euler Equations," AIAA Paper No. 85-0122, January 1985.

7. Gapcynski, J. P. and Carlson, H. W., "A Pressure-Distribution Investigation of the Aerodynamic Characteristics of a Body of Revolution in the Vicinity of a Reflection Plane at Mach Numbers of 1.41 and 2.01," NACA RM L54J29, no date given.

8. Mastin, C. Wayne, "Numerical Solution of the Euler Equations on Dynamic Grids," Final Report, USAF-SCEEE Research Initiation Program, Subcontract Number 83 RIP 10, August 1984.

END

DtiC

7 — 86